UC Riverside

UC Riverside Previously Published Works

Title

Putative Coiled-Coil Domain-Dependent Autoinhibition and Alternative Splicing Determine SHTN1's Actin-Binding Activity

Permalink

https://escholarship.org/uc/item/7wx4z7ph

Journal

Journal of Molecular Biology, 432(14)

ISSN

0022-2836

Authors

Ergin, Volkan
Zheng, Sika

Publication Date

2020-06-01

DOI

10.1016/j.jmb.2020.04.025

Peer reviewed

HHS Public Access
Author manuscript
J Mol Biol. Author manuscript; available in PMC 2021 June 26.

Putative coiled-coil domain-dependent autoinhibition and alternative splicing determine SHTN1's actin-binding activity

Volkan Ergin[§], **Sika Zheng**[#]

Division of Biomedical Sciences, University of California, Riverside, Riverside, CA 92521, USA

Abstract

The actin cytoskeleton plays a pivotal role in cell development, morphogenesis, and other cellular functions. Precise control of actin dynamics requires actin-binding proteins (ABPs). Here, we characterize multifarious regulation of SHTN1 (shootin1) and show that, unlike known ABPs, SHTN1's actin binding activity is intrinsically inhibited by a putative coiled-coil domain (CCD) and the autoinhibition is overcome by alternative splicing regulation. We found SHTN1 contains a noncanonical WH2 domain and an upstream proline rich region (PRR) that by themselves are sufficient for actin interaction. Alternative splicing of *Shtn1* at the C terminus and downstream of the WH2-PRR domain produces a long (SHTN1L or shootin1 b) and a short (SHTN1S or shootin1 a) isoform, which both contain the described PRR and WH2 domains. However, SHTN1S does not interact with actin due to inhibition mediated by an N-terminal CCD. A SHTN1L-specific C-terminal motif counters the intramolecular inhibition and allows SHNT1L to bind actin. A nuclear localization signal is embedded between PRR and WH2 and is subject to similar autoinhibition. SHTN1 would be the first WH2-containing molecule that adopts CCD-dependent autoinhibition and alternative splicing-dependent actin interaction.

Graphical abstract

[#]**Correspondence to Sika Zheng:** Division of Biomedical Sciences, School of Medicine, University of California, Riverside, Riverside, CA 92521, USA; sika.zheng@ucr.edu; Tel. 1-951-827-7670; Fax. 1-951-579-4118.
[§]**Present address:** Department of Otolaryngology, Harvard Medical School and Massachusetts Eye and Ear Infirmary, Boston, MA 02114, USA.
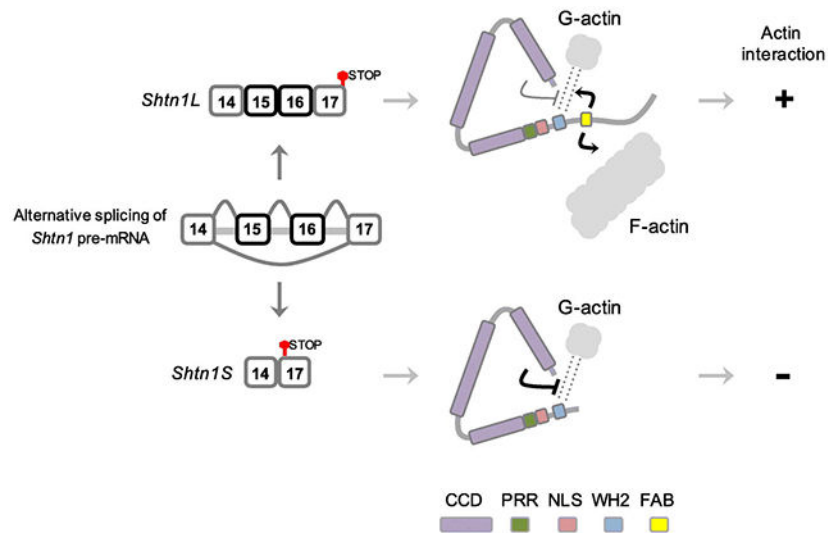
Author Contributions
V.E. and S.Z. conceptualized the project. V.E. conducted the experiments and analyzed the data. V.E. and S.Z. wrote the original draft. S.Z. revised and edited the manuscript.

Conflict of interest
The authors have declared that no competing interests exist.

CCD PRR NLS WH2 FAB

Introduction

Organization and regulation of the cytoskeleton play important roles in cellular proliferation, differentiation, adhesion and cell migration [1,2]. Actin, the major component of the cytoskeleton, exists in two different states: globular monomeric G-actin and filamentous oligomeric F-actin. Rapid assembly and disassembly of the actin cytoskeleton control cell motility, endocytosis, and functional polarity [3]. Ensuring normal actin cytoskeleton dynamics requires the actin-biding proteins (ABP). Actin doesn't function in a naked state but requires a plethora of molecular partners (i.e., ABPs) to orchestrate actin dynamics. ABPs are common targets of extra- and intracellular signaling cascades to govern actin filament nucleation, elongation, capping, crosslinking, and monomer sequestration [4]. Identification and characterization of new actin binding molecules can shed light on actin biology and provide new molecular handles to understand and manipulate cellular processes.

Most ABPs can be grouped by their domain compositions (e.g., Wiskott–Aldrich syndrome protein homology domain-2 (WH2), actin-depolymerizing factor/cofilin (ADF/cofilin) domain, gelsolin-homology domain, calponin-homology (CH) domain, and myosin motor domain) [3]. WH2, found in β-thymosins, Ena/VASP, inverted formin 2, Spire, Cobl, and Arp2/3 complex activators (WASP, WASH, WHAMM, WAVE, etc.), is one of the most represented actin-binding motifs. The WH2 domain, in either single module or tandem repeats, binds actin monomers and assists in filament assembly or actin sequestration [5–7]. WH2 can act along with proline-rich regions (PRR), which bind profilin and other signaling/regulatory proteins (e.g., SH3 domain-containing proteins). PRR serves as the loading dock for the profilin-actin complex to increase the local concentration of actin monomers and

accelerates incorporation of ATP-bound monomers to the growing end of actin filaments [8–10].

Neuronal morphogenesis critically relies on actin dynamics [11]. Early axonogenesis is coordinated by a neuron-specific alternative splicing program in genes largely regulating cytoskeleton dynamics [12–15]. One example is *Shtn1*. The *Shtn1* short isoform (*Shtn1S*) lacks exons 15 and 16; inclusion of these two exons alters the C terminus and produces the *Shtn1L* long isoform [16]. SHTN1S was originally identified as a neuronal polarity gene induced at the early stage of axon formation [17]. The increase in SHTN1S is due to *Shtn1* pre-mRNA switching splicing from SHTN1L to SHTN1S [12]. While SHTN1L promotes axon growth [12]. SHTN1S induces axon specification [17], indicating that axon growth and specification may be intrinsically coupled through alternative splicing regulation [18]. We have previously shown that SHTN1L, but not SHTN1S, interacts with F-actin thanks to a necessary F-actin binding motif encoded by exon 15 [12].

In the present study, we found the F-actin-binding motif is insufficient for actin interaction, suggesting other auxiliary regions must be involved. We identified a single noncanonical WH2 domain and a PRR domain in SHTN1L that, in and of themselves, are sufficient for actin binding. Interestingly, the WH2 and PRR domains are within the common region of SHTN1S and SHTN1L, but SHTN1S exhibits no actin binding activity. We further found multiple putative coiled-coil domains (CCD) in SHTN1, one of which exerts intramolecular autoinhibition of actin binding. Only through alternative splicing of the C terminus is autoinhibition alleviated.

Results

SHTN1L interaction with actin depends on its WH2 domain

Shtn1L and *Shtn1S* encode the same N-terminal sequence but different C termini (Fig. 1a). Shtn1L's unique C terminus possesses a sequence motif (FAB or simply F) that contains a polybasic sequence (RRRK) necessary for F-actin interaction [12]. When the consecutive arginine residues are mutated to glycine, a SHNT1L$^{RRR>GGG}$ mutant fails to bind cellular actin or *in vitro* pre-formed actin filaments [12]. This observation led us to ask whether the unique C terminus of SHNT1L (1L-C-term) is by itself sufficient for binding actin. We performed co-IP assays using N2a cells expressing EGFP-fused SHTN1L, SHTN1S, or the 1L-C-term fragment. The 1L-specific C-terminus did not pull-down endogenous actin as SHTN1L did (Fig. 1b), suggesting additional motifs were needed for actin binding.

We retrieved functional sites predicted by ScanProsite [19] and ELM [20]. With loosened criteria, the tools found putative PRR and WH2 domains encoded by exons 11 and 13, respectively. These candidate motifs are 100% identical between humans and rodents (Fig. S1). Independent *in silico* analyses separately suggested the existence of a PRR [17] and WH2 domain [21] within SHTN1, but these predictions were not experimentally tested. The presumed WH2 motif appears phylogenetically distant, containing only a few residues shared by other well-known WH2 domains (Fig. 1c **and** S2). We therefore consider the SHTN1-WH2 domain a non-canonical WH2 domain. We did *in silico* modeling and found

the SHTN1-WH2 domain nevertheless structurally resembles other known WH2 domains (Fig. S3).

To test whether these predicted domains are functional, we performed co-IP in N2a cells expressing EGFP-fused PRR, WH2, or PRR-WH2 fragment. PRR alone pulled down profilin (PFN2) but not actin. WH2 alone pulled down actin but not PFN2 (Fig. 1d). Since profilin is an actin-monomer binding protein, these results confirmed the stringency of the co-IP experiment to identify direct interacting partners. Importantly, interactions with actin and PFN2 were both substantially enhanced when PRR-WH2 was expressed. These results agreed with the idea that profilin transfers actin to WH2 and that WH2-actin interaction is enhanced in the presence of PRR [9,22,23].

To assess contributions of individual domains to SHTN1L's actin-binding, we created EGFP-fused mutant constructs of WH2 (1L-WH2-m; LRPV>GAAG, 423-426 aa) and FAB regions (1L-FAB-m; RRR>GGG, 482-484 aa), respectively (Fig. 1a). Both mutants showed substantially weaker and sometimes undetectable interaction with cellular actin compared to wild-type SHTN1L (Fig. 1e), suggesting both regions are necessary for actin interaction *in vivo*.

To exclude possible confounding factors in the co-IP experiments, we tested SHTN1's direct interaction with actin monomers by G-actin binding assay [24,25]. Briefly, EGFP-SHTN1 variants were immunopurified via GFP-Trap beads and washed in a stringent buffer to eliminate interactions with endogenous actin and re-equilibrated in G-buffer (5 mM Tris.HCl pH 8.0, 0.2 mM $CaCl_2$, 0.2 mM ATP, 0.5 mM DTT, see Materials and Methods). Meanwhile, G-actin resuspended in G-buffer was cleared by ultracentrifugation to remove actin oligomers (Fig. S4). The supernatant containing ATP-actin monomers was immediately incubated with the SHTN1 variants immobilized on beads in G-buffer. We found that full-length SHTN1L, but not SHTN1S, directly interacts with G-actin *in vitro* and that WH2 or FAB mutants substantially reduce interaction with actin monomers (Fig. 1f). Therefore, WH2 domain and FAB region concertedly enhance actin-binding activity of SHTN1L.

SHTN1S is autoinhibited by the N-terminal putative coiled-coil domain

Despite containing the PPR and WH2 domains, SHTN1S does not interact with actin (Fig. 1a, 1b, 1e, and 1f). This raises the possibility that the WH2-actin interaction is inhibited for SHNT1S. We noticed that the WH2 domain is located at the very C terminus of SHNT1S and hypothesized that autoinhibition, if any, might originate from the N terminus (Fig. 1a). *In silico* predictions proposed that N-terminus of SHTN1S had three distinct putative coiled-coil domains (CCD) [17]. Our analysis based on Marcoil algorithm [26] agreed on the presence of CCDs (herein referred to as CCD-I, CCD-II and CCD-III) upstream of the WH2 domain, despite slight differences regarding the boundaries of each CCD from the previous prediction (Fig. 2a).

To evaluate the contributions of CCDs to silencing the WH2 domain in SHTN1S, we created N-terminal EGFP-fused expression vectors with sequential deletions of the three CCDs (Fig. 2b). We performed co-IP experiments and found that the SHTN1S WH2 domain became

activated when the first CCD was deleted (Fig. 2c). Further deletion of CCD-II still enhanced SHTN1S interacting with actin. These data showed that WH2 in SHTN1S is inert to bind actin because of autoinhibitory regulation from the N-terminal CCD-I (and possibly CCD-II).

This observation led us to ask whether CCDs also influence the actin binding activity of SHNT1L, since SHTN1L possesses the same domains (Fig. 2d). We tested SHTN1L's interaction with actin by sequentially removing the three CCDs using co-IP (Fig. 2e). CCD-I deletion consistently promoted the actin binding activity of SHTN1L (Fig. 2f) but continual deletion had no further effect. These data demonstrate that CCD-I functions as the major autoinhibitory module.

We evaluated direct interaction of deletion mutants with G-actin using the previously described G-actin binding assay. Consistent with *in vivo* data, this assay showed CCD-I deletion enhances interaction with G-actin substantially for SHTN1S and to a less degree for SHTN1L (Fig. 2g). Collectively, our findings revealed an autoinhibitory mechanism using N-terminal CCD-I to restrain actin-binding activities of SHTN1 isoforms.

Removal of CCD promotes SHTN1L binding to F-actin

We subsequently tested whether the CCD deletion mutants would affect F-actin binding using F-actin co-sedimentation assays and purified FLAG-tagged SHTN1L variants. In bacteria, recombinant GST- or His-tagged SHTN1 proteins were mostly pelleted in insoluble fraction and highly degraded. We therefore purified recombinant SHTN1 proteins from mammalian (N2a) cells using FLAG-tag affinity purification. Coomassie brilliant blue staining confirmed the purity of the FLAG-tagged targets (Fig. 3a).

For co-sedimentation assays, we incubated individual 250 nM FLAG-tagged target proteins with *in vitro* pre-formed actin filaments, which were subsequently pelleted by ultracentrifugation. SHTN1L variants were not self-pelleted in the absence of actin (Fig. S5). In the presence of actin, SHNT1L became co-pelleted with F-actin and some (−50%) remained in supernatant (Fig. 3b and 3c). We tested whether CCD-I inhibited Shtn1L's binding to F-actin, and found 1L- CCD-I and 1L- CCD-I-II were almost completely associated with F-actin (Fig. 3b and 3c). 1L- CCD-I-II-III and actin co-migrate at 42 kDa in SDS-PAGE. 1L- CCD-I-II-III cannot be separated from actin in Coomassie blue-stained SDS-PAGE gel (Fig. 3b lower panel). We used fluorescent Western blots to distinguish the two proteins and the background signals of 1L- CCD-I-II-III (light grey bands) were due to leakage of actin fluorescent signals during Typhoon scanning. We found 1L- CCD-I-II-III molecules in the supernatant with a ratio similar to the full-length protein, suggesting CCD-III was not part of the inhibitory module. We note that, compared to 1S- CCD-I-II, 1S- CCD-I-II-III showed reduced binding to cellular and monomeric actin (Fig. 2c and 2g, see Discussion).

We incubated increasing concentrations of SHTN1L or 1L- CCD-I with pre-assembled F-actin (2 μM total actin input) for further comparison. The maximal final concentration we could obtain of SHTN1 proteins (from mammalian cells) in the cosedimentation assay was 0.6 μM. 1L- CCD-I exhibited a clear shift towards bound-state compared to the SHTN1L

full-length protein (Fig. 3d and 3e). We estimated the *Kd* values by curve fitting from the data without saturation. The affinity of 1L- CCD-I for F-actin was much stronger than that of SHTN1L, with the dissociation constant (*Kd*) found to be 21.86 nM and 164.3 nM, respectively (Fig. 3e). Overall, this result shows that CCD-I restrains SHTN1L's F-actin binding activity.

SHTN1 has a nuclear localization signal embedded between PRR and WH2 domain

We found some of the CCD-deletion mutants, when expressed in cells, were enriched in nuclei in contrast to the cytoplasmic full-length isoform proteins. Nuclear accumulation of the SHTN1S N-terminus deletion mutant was previously noted but not quantified, and the underlying mechanism remained unknown [27]. We therefore quantitatively determined the relationship between CCDs and nuclear localization of SHTN1. For SHTN1S, CCD-I led to either complete nuclear localization or diffuse distribution between the cytosol and nucleus. Deletion of CCD-I and II further induced nuclear translocation of the mutant SHTN1S protein (Fig. 4a and 4b). For SHTN1L, CCD-I deletion did not significantly change cellular localization of the protein. However, a clear shift toward nuclear localization was observed upon deletion of CCD-I and II (Fig. 4c and 4d). Deletion of all three CCDs resulted in nuclear retainment of both isoforms. We have not found any nuclear export signal in the deleted CCD regions.

Following the findings that CCD inhibits SHTN1's actin-related activity, we suspected SHTN1 possessed a nuclear localization signal (NLS) masked by the CCD domains. Using the seqNLS prediction tool [28], we found a conserved putative NLS buried between the PRR and WH2 domains (Fig. 4e and 4f). To test the activity of this NLS motif, EGFP-fused PRR, WH2 domain, and PRR-WH2 domain constructs were expressed in cells. EGFP-PRR and EGFP-WH2 fragments were equally distributed in the nucleus and cytoplasm, whereas the EGFP-PRR-WH2 fragment containing the putative NLS was observed solely in the nucleus (Fig. 4g). Therefore, although small molecules (less than 50 kDa) shuttle freely between nucleus and cytosol through nuclear pores [29], the proposed NLS signal embedded between PRR and WH2 in EGFP-PRR-WH2 fragment sufficiently induces nuclear localization activity. We mutated the putative motif (PRR-WH2$^{RKR>GGG}$, 378-380 aa) and found the GFP-fused mutant is exclusively retained in the cytosol (Fig. 4e–g), proving the motif is necessary for nuclear trans-localization. Since PRR-WH2 (RKR>GGG) is less than 40 kDa, its enrichment in the cytoplasm might be due to its binding to cytoplasmic actin molecules. These results show that the NLS, like the adjacent WH2 motif, is subject to inhibition imposed by the CCD regions.

SHTN1L interacts with F-actin *in vivo*

SHTN1L (but not SHTN1S) is endogenously expressed in N2a cells (Fig. S6a). To further determine whether SHTN1L interacts with F-actin *in vivo*, we examined SHTN1L's subcellular localization in N2a cells using immunocytochemistry and phalloidin staining. We observed that endogenous SHTN1L proteins in N2a cells strongly colocalize with phalloidin-stained F-actin, particularly across cellular edges of lamellipodia (Fig. S6b).

We tested whether EGFP-fused SHTN1L- CCD-I (N terminus CCD1 deletion) and SHTN1S (C terminus deletion) exhibited differential actin colocalization than SHTN1L in cells to determine which would affect F-actin colocalization. EGFP-SHTN1L showed actin-colocalization as endogenous SHTN1L. Therefore, EGFP fusion did not obviously alter SHTN1L's location. We also found EGFP-SHTN1L could induce F-actin-enriched bundle-like aggregates at cellular edges, possibly due to its ability of promoting actin polymerization (Fig. S7a). By contrast, EGFP-SHTN1S, like EGFP control, did not exhibit obvious F-actin colocalization at cellular edges (Fig. S7b). On the other hand, EGFP-1L- CCD-I strongly localized within F-actin-rich areas (Fig. S7c). These *in vivo* observations are consistent with biochemical characterization of SHTN1 protein variants regarding their binding to F-actin.

Discussion

The WH2 domain in SHTN1 is noncanonical. To date, WH2 domains are found in >60 modular proteins [30]. By primary sequences the SHTN1-WH2 domain is distantly related to WH2 domains of other well-known ABPs. Only 4 of 8 consensus WH2 residues (LL××l××G××LKKV) are found in SHTN1, partially explaining why SHTN1 has not been characterized as an ABP. Nevertheless, the SHTN1-WH2 domain displays a similar secondary structure to known WH2 domains: an N-terminal α-helix followed by an extended C-terminal region (Fig. S3). Identification of this non-canonical WH2 domain may spur prediction and discovery of even more WH2-containing ABPs. The latest WH2-containing proteins were identified in the 2000s [31], as the pace of ABP discovery slowed down. Discovery of a new ABP often leads to new knowledge of actin biology [32]. Therefore, identification of a new actin binding protein and characterization of its domains is significant.

PRR, WH2 domain and FAB sites concertedly enhance SHTN1L interaction with actin.

Several WH2-containing ABPs adopt various auxiliary motifs to facilitate actin binding. Formin proteins such as INF2, mDIA1, FMNL3, and DAAM1 contain formin-homology (FH) 1 and 2 domains in juxtaposition. The FH1 domain is essentially PRR. The FH2 domain, dissimilar from the SHTN1 FAB motif, cooperates with the formin WH2 domain to recruit actin monomers and elongate filaments [31]. For Arp2/3 complex activators (WASP, WAVE, *etc.*), the central (C) and acidic (A) domains synergize with WH2 for actin nucleation [33].

The SHTN1L WH2 domain by itself exhibits moderate actin interaction, which is enhanced by upstream PRR and downstream FAB sites. In this sense, the tripartite (PRR-WH2-FAB) domain arrangement of SHTN1L is somewhat reminiscent of Ena/VASP molecules. VASP recruits profilin-actin monomers through its PRR and delivers the actin monomer to the G-actin binding domain (i.e. WH2) to drive filament elongation [33,34], while its FAB site provides an anchor point to the barbed end of the actin filament [9]. The transition of an actin monomer from the WH2 domain to the barbed end triggers stepping of VASP on the elongating barbed ends [33]. However, this similarity cannot be extrapolated to predict a

protein's precise activity in a cellular context as domains outside of PRR-WH2-FAB may be as important.

CCD-I dependent autoinhibition regulates SHTN1 activity

WH2-containing SHTN1S is inert to actin binding thanks to autoinhibitory regulation from the N-terminal CC domain. Deletion of CCD-I allows SHNT1S to interact with actin. Similarly, CCD-I deletion enhances SHTN1L's actin binding. Therefore, CCD-I likely masks the C-terminal PRR-WH2 region from actin interaction.

Autoinhibition is supported by nuclear translocation of SHTN1 mutants. We found that SHTN1 carries a normally silent NLS motif buried between the PRR and WH2 domains. Adjacent to WH2, the NLS motif is masked by the N-terminal CC domains in a naive state, preventing nuclear translocation. Deletion of the CC domains exposes the NLS motif, allowing nuclear localization of SHTN1 proteins. We observed that SHTN1L is more prone to staying in cytosol than SHTN1S, which might be caused by the F-actin-bound state of SHTN1L. Whether and how nuclear localization of SHTN1 and its actin-related activity are functionally coupled will be interesting to explore in future studies, since nuclear actin dynamics are important for transcriptional regulation and DNA-damage response [35–38].

The CCD-III domain appeared to influence SHNT1L and SHTN1S differently. For cellular actin and G-actin, CCD-III deletion led to less actin binding for SHTN1S but had a marginal effect on SHTN1L (Fig. 2c and 2g). One possible explanation is that CCD-III, located at the immediate N terminal extension of PRR-NLS-WH2, stabilizes SHTN1S interaction with cellular actin and G-actin. The SHNTIL-specific C-terminus (FAB site) may have the same stabilizing effect as CCD-III in a non-addictive manner, thereby occluding any CCD-III effect on SHTN1L. SHTN1L binding to G-actin is therefore less dependent on CCD-III. In line with this notion, FAB mutation of the full-length SHTN1L reduced interaction with cellular actin and G-actin (Fig. 1e and 1f). Interestingly, although not affecting SHTN1L's interaction with G-actin, CCD-III deletion reduced SHTN1L's binding to F-actin (Fig. 3c).

SHTN1 differs among WH2-domain-containing molecules for containing a putative coiled-coil domain as a regulatory motif of its actin-binding activity and for overcoming autoinhibition through alternative splicing. Other ABPs adopt different autoinhibition mechanisms, which often require a third protein as a regulatory factor. For espin 1, the N-terminal ankyrin repeat domain interacts with the ankyrin repeat-binding peptide near the actin-binding site; Myosin III reverses the autoinhibition by binding the ankyrin repeat domain [39]. In formins containing a WH2 or WH2-like domain (e.g., FMNL3 or mDIA1 [31,40]), the autoinhibitory conformation results from intramolecular interaction between its dimerization domain (DID) and diaphanous autoregulatory domain (DAD). Binding of Rho family GTPases to the N terminus GTPase-binding domain (GBD) of formin disrupts autoinhibition and thus activates the formin homology-2 (FH2) domain to recruit actin monomers [41,42]. In WASP, another ABP possessing WH2 domain, autoinhibition is mediated by intramolecular binding of the GTPase binding domain (GBD) to the C-terminal W/C/A (WH2/Central/Acidic) region, which makes WH2 inaccessible. This intramolecular inhibition is freed when Cdc42 binds the Cdc42/Rac interactive binding (CRIB) motif, leading to interaction with G-actin and Arp2/3 complex [43,44]. Interestingly, Cdc42 and

Rac1 GTPases promote PAK1-mediated SHTN1S phosphorylation at Ser101 and Ser249 [45]. These phosphorylation sites reside in CCD-I and CCD-II, respectively, and might play a role in regulating the autoinhibition.

In conclusion, we show that SHTN1 adopts multi-modality of regulation, including alternative splicing, intramolecular cooperation, and autoinhibition to influence its biological activities. The actin-binding activity of SHTN1 is autoinhibited by its N-terminal putative coiled-coil domain and disinhibited via alternative splicing regulation at its own C-terminus. Besides altering actin interaction, this regulation could induce isoform-specific subcellular localization of SHTN1 proteins to further modulate SHTN1's functions.

Materials and Methods

Cell culture and transfection

N2a cells (mouse neuroblastoma, ATCC #CCL-131) were cultured in DMEM supplemented with 10% USDA-FBS and 2 mM GlutaMAX (Thermo). DNA plasmids were constructed using pEGFP-C1 and pCAGIG [12], and delivered to cells by GeneTran-III (BioMiga).

Recombinant DNA constructs

As described, pEGFP-C1 and pCAGIG were used as host vectors [12]. Briefly, coding sequences were inserted in pEGFP-C1 or pCAGIG vectors linearized by Xhol-TspMI and Xhol-Notl enzymes (NEB), respectively. Primer sequences used for these constructs are shown in Table S1. All constructs were confirmed by Sanger sequencing prior to transfections. Plasmids were propagated in DH5a *E. coli* cells and prepared using Miniprep kits (Qiagen).

Site-directed mutagenesis

Conversion mutants (PRR-WH2, RKR>GGG, 378-380 aa; 1L-WH2-mut, LRPV>GAAG, 423-426 aa; 1L-FAB-mut, RRR>GGG, 482-484 aa) were made by PCR amplification of expression plasmids *in vitro* to incorporate mutagenic nonoverlapping primers. Plasmids were subjected to Dpnl (NEB) digestion to eliminate non-mutated templates. The resulting plasmid was transformed into DH5a *E. coli* and cloned. Primers used for site-directed mutagenesis are shown in Table S1.

Co-immunoprecipitation and immunoblotting

N2a cells overexpressing EGFP-fused target molecules were lysed in 1 ml buffer containing 50 mM Tris.HCI pH 7.4, 150 mM NaCl, 0.5% Triton X-100, inhibitor cocktails (Roche), 1 mM PMSF, and 100U/ml Turbonuclease (Sigma). Lysates were cleared by centrifugation at 17,000 *g* for 15 min at 4°C and incubated with 12 μl GFP-Trap magnetic beads (Chromotek) for 1 h at 4°C with gentle rotation. Beads were washed three times with 1 ml buffer containing 50 mM Tris.HCI pH 7.4, 300 mM NaCI, 0.5% Triton X-100, 1 mM PMSF. Bead-bound proteins were denatured by boiling in 15 μl sample buffer before SDS-PAGE. Ten μl of the boiled-sample was loaded for probing with target antibodies. Five μl of the samples was used to probe with GFP antibody as expression control. Total protein lysate and IP fractions were analyzed by immunoblotting using primary antibodies against β-Actin

(sc-47778, SCBT), Profilin-2 (sc-100955, SCBT), GFP (GFP-1020, AvesLab), FLAG M2 (F3165, Sigma) and SHTN1 (kindly provided by Dr. O. Reiner) [46]. Primary antibodies were detected by appropriate fluorophore-conjugated secondary antibodies (donkey anti-mouse IgG Alexa Fluor 647, donkey anti-rabbit IgG Alexa Fluor 568 or goat anti-chicken IgG Alexa Fluor 488; Thermo). Blots were visualized by Typhoon FLA9000.

Protein purification

Multiple attempts to purify His- or GST-tagged SHTN1 variants from bacteria failed because SHTN1 proteins were highly degraded and pelleted in insoluble fractions. We therefore used FLAG-tag affinity purification with transiently transfected mammalian cells (N2a). Briefly, FLAG-tagged constructs were individually transfected into N2a cells cultured in 15-cm dishes. Forty-eight hours after transfection, cells were lysed in 5 ml buffer containing 50 mM Tris.HCl pH 7.4, 500 mM NaCl, 1 mM EDTA, 1% Triton X-100, inhibitor cocktails, 1 mM PMSF, and 100U/ml Turbonuclease. Lysates were cleared by centrifugation at 17,000 g for 15 min at 4°C. For affinity purification, 200 μl slurry of anti-FLAG M2 magnetic beads (Sigma) equilibrated in lysis buffer were added into centrifuge-cleared cell lysate and incubated for 3 h at 4°C. We collected beads on a magnetic rack and washed the beads three times with 2 ml lysis buffer. Bound proteins were eluted twice at RT for 15 min with 1 ml elution buffer containing TBS buffer (10 mM Tris.HCl pH 7.4, 100 mM NaCl) supplemented with 200 μg/ml 3X FLAG-peptide (Apex Bio). Eluted proteins were concentrated and washed with TBS buffer using Amicon Ultra centrifugal filters (MWCO 30 kDa). Concentrated proteins and BSA standards were analyzed by SDS-PAGE stained with coomassie blue G-250 dye (G-Biosciences) to calculate molar concentration of target molecules.

G-actin binding assay

This assay was carried out with minor modifications [24,25]. N2a cells overexpressing EGFP-fused SHTN1 variants were lysed in a buffer containing 50 mM Tris.HCl pH 7.4, 1 M NaCl, 1 mM EDTA, 1% Triton X-100, 1 mM PMSF, inhibitor cocktails, and 100U/ml Turbonuclease. Lysates were cleared by centrifugation at 17,000 g for 15 min at 4°C. Centifuge-cleared cell lysates were incubated with 20 μl GFP-Trap magnetic beads for 1 h at 4°C with gentle rotation. Protein-bound beads were then washed six times with 1 ml lysis buffer to remove interaction with endogenous actin, followed by equilibration in 1 ml G-buffer (5 mM Tris.HCl pH 8.0, 0.2 mM $CaCl_2$, 0.2 mM ATP, 0.5 mM DTT). Half the bead volume (10 μl) was kept as negative controls. The other half (10 μl) was used for testing G-actin binding as below. Briefly, one aliquot (10 μl, 10 mg/ml) of human platelet actin was diluted in 340 μl G-buffer and incubated on ice for 1 h. This aliquot (6 μM) was centrifuged for 1 h at 70,000 rpm (TLA100; Beckman) to remove actin oligomers. Fifty μl of the −350 μl supernatant containing monomeric ATP-actin was transferred to the second half volume (10 μl) of GFP-Trap beads and individually incubated in 500 μl G-buffer for 1 h at 4°C. Beads on a magnetic rack were washed three times with 1 ml G-buffer plus 0.1% Triton X-100. Proteins bound to beads were released by boiling, and subjected to immunoblotting with mouse anti-p-actin and chicken anti-GFP primary antibodies, respectively. Then membranes were incubated with donkey anti-mouse IgG Alexa Fluor 647 and goat anti-chicken IgG Alexa Fluor 488 secondary antibodies (Thermo) at RT for 1 h and visualized by

Typhoon FLA9000. At 5°C, in the absence of Mg^{2+} and KCI, the critical concentration of ATP and Ca^{2+}-bound platelet-derived actin is about 3 mg/ml (−60 μM) [47], which is 100 times higher than the final concentration of actin molecules (0.6 μM) we used in this experiment. Therefore, actin molecules wouldn't have polymerized under the conditions described above.

Actin cosedimentation assay

A non-muscle actin isotype was used based on our *in vivo* data obtained from a non-muscle mammalian (N2a) cell line. A frozen aliquot of human platelet actin protein (Cytoskeleton, APHL99) was diluted in G-buffer and incubated for 1 h on ice. Actin filaments were formed by adding 0.1 volume of 10X polymerization buffer (100 mM Tris.HCI pH 7.5, 500 mM KCI, 20 mM $MgCI_2$ and 10 mM ATP) (Cytoskeleton, BSA02) followed by RT incubation for 1 h. Purified FLAG-tagged SHTN1 proteins were incubated with actin filaments for 30 min at RT. Actin filaments with bound proteins were pelleted by ultracentrifugation at 70.000 rpm for 1 h at RT. Equal amounts of pellet and supernatant fractions mixed with 4X sample buffer were boiled and resolved by SDS-PAGE. The target proteins were visualised using coomassie staining or immunoblotting with anti-FLAG and anti-β-actin mAbs. Blots were visualized by Typhoon FI_A9000 and band intensities were quantified by ImageJ (NIH).

To determine a dissociation constant (*Kd*), increasing amounts (0.018, 0.037, 0.075, 0.15, 0.3, and 0.6 μM) of FLAG-SHTN1L and SHTN1L- CCD-I were incubated with 2 μM preassembled F-actin for 30 min at RT as described above. After centrifugation at 70.000 rpm for 1 h at RT, equal amounts of the supernatants and pellets were individually subjected to SDS-PAGE. The target proteins were detected using coomassie staining or immunoblotting with anti-FLAG and anti-β-actin mAbs as stated above. The amounts of test molecules in the pellet and supernatant were quantified by ImageJ using immunoblot images. A *Kd* value for SHTN1L and SHTN1L- CCD-I bound to actin was calculated by fitting the data of protein bound versus protein free [48,49] to a nonlinear function with one-site specific binding [50] using GraphPad Prism package (version 8.3.1).

Immunofluorescence

Cells were fixed in 4% PFA for 10 min, permeabilized with ice-cold PBS containing 0.3% Triton X-100 (PBST) for 5 min, and blocked in PBST buffer containing 5% donkey serum, 2% BSA, 0.02% NaN_3 for 1 h at RT. Cells were stained with polyclonal anti-GFP or anti-SHTN1 antibodies diluted in blocking buffer overnight at 4°C, followed by an 1 h incubation at RT with fluorophore-conjugated 2°Ab, phalloidin and DAPI for nuclei staining. Coverslips were mounted with ProLong mountant (Thermo) prior to imaging. Images were captured with a Nikon DS-Qi2 camera mounted on a Nikon Eclipse Ci microscope.

Statistical analyses

All experiments were performed at least three times. Statistical analysis was performed with the Student's t-test using Microsoft Excel. For data presented as counts in a 2×2 table, we

used Fisher's exact test. Values were expressed as mean ± SEM. To be considered statistically significant, p values had to be less than 0.05.

Supplementary Material

Refer to Web version on PubMed Central for supplementary material.

Acknowledgments

Abbreviations used:

WH2	Wiskott-Aldrich syndrome protein homology domain-2
PRR	proline-rich region
FAB	F-actin binding site
CCD	coiled-coil domain
ABP	actin-binding protein
NLS	nuclear localization signal
SHTN1L	shootinl isoform 1 (long isoform)
SHTN1S	shootinl isoform 2 (short isoform)

References

[1]. Suetsugu S, Takenawa T, Regulation of cortical actin networks in cell migration, Int. Rev. Cytol 229 (2003) 245–86. [PubMed: 14669958]

[2]. Qualmann B, Kessels MM, Kelly RB, Molecular links between endocytosis and the actin cytoskeleton, J. Cell Biol 150 (2000). doi: 10.1083/jcb.150.5.F111.

[3]. Dominguez R, Actin-binding proteins - A unifying hypothesis, Trends Biochem. Sci 29 (2004) 572–578. doi:10.1016/j.tibs.2004.09.004. [PubMed: 15501675]

[4]. Lee SH, Dominguez R, Regulation of actin cytoskeleton dynamics in cells., Mol. Cells 29 (2010) 311–25. doi: 10.1007/s10059-010-0053-8. [PubMed: 20446344]

[5]. Ahuja R, Pinyol R, Reichenbach N, Custer L, Klingensmith J, Kessels MM, Qualmann B, Cordon-bleu is an actin nucleation factor and controls neuronal morphology., Cell. 131 (2007) 337–50. doi:10.1016/j.cell.2007.08.030. [PubMed: 17956734]

[6]. Bosch M, Le KHD, Bugyi B, Correia JJ, Renault L, Carlier MF, Analysis of the Function of Spire in Actin Assembly and Its Synergy with Formin and Profilin, Mol. Cell 28 (2007) 555–568. doi:10.1016/j.molcel.2007.09.018. [PubMed: 18042452]

[7]. Didry D, Cantrelle FX, Husson C, Roblin P, Moorthy AME, Perez J, Le Clainche C, Hertzog M, Guittet E, Carlier MF, Van Heijenoort C, Renault L, How a single residue in individual β-thymosin/WH2 domains controls their functions in actin assembly, EMBO J. 31 (2012) 1000–1013. doi: 10.1038/emboj.2011.461. [PubMed: 22193718]

[8]. Kovar DR, Harris ES, Mahaffy R, Higgs HN, Pollard TD, Control of the assembly of ATP- and ADP-actin by formins and profilin, Cell. 124 (2006) 423–435. doi:10.1016/j.cell.2005.11.038. [PubMed: 16439214]

[9]. Ferron F, Rebowski G, Lee SH, Dominguez R, Structural basis for the recruitment of profilin-actin complexes during filament elongation by Ena/VASP, EMBO J. 26 (2007) 4597–4606. doi: 10.1038/sj.emboj.7601874. [PubMed: 17914456]

[10]. Chereau D, Kerff F, Graceffa P, Grabarek Z, Langsetmo K, Dominguez R, Actin-bound structures of Wiskott-Aldrich syndrome protein (WASP)-homology domain 2 and the implications for filament assembly., Proc. Natl. Acad. Sci. U. S. A 102 (2005) 16644–9. doi:10.1073/pnas.0507021102. [PubMed: 16275905]

[11]. Dent EW, Gertler FB, Cytoskeletal dynamics and transport in growth cone motility and axon guidance., Neuron. 40 (2003) 209–27. doi:10.1016/s0896-6273(03)00633-0. [PubMed: 14556705]

[12]. Zhang M, Ergin V, Lin L, Stork C, Chen L, Zheng S, Axonogenesis Is Coordinated by Neuron-Specific Alternative Splicing Programming and Splicing Regulator PTBP2, Neuron. 101 (2019) 690–706.e10. doi: 10.1016/j.neuron.2019.01.022. [PubMed: 30733148]

[13]. Vuong CK, Black DL, Zheng S, The neurogenetics of alternative splicing, Nat. Rev. Neurosci 17 (2016) 265–281. doi:10.1038/nrn.2016.27. [PubMed: 27094079]

[14]. Zheng S, Alternative splicing and nonsense-mediated mRNA decay enforce neural specific gene expression, Int. J. Dev. Neurosci 55 (2016) 102–108. doi:10.1016/j.ijdevneu.2016.03.003. [PubMed: 26968265]

[15]. Zheng S, Black DL, Alternative pre-mRNA splicing in neurons: Growing up and extending its reach, Trends Genet. 29 (2013) 442–448. doi: 10.1016/j.tig.2013.04.003. [PubMed: 23648015]

[16]. Ergin V, Erdogan M, Menevse A, Regulation of Shootinl Gene Expression Involves NGF-induced Alternative Splicing during Neuronal Differentiation of PC12 Cells, Sci. Rep 5 (2015). doi: 10.1038/srep17931.

[17]. Toriyama M, Shimada T, Kim KB, Mitsuba M, Nomura E, Katsuta K, Sakumura Y, Roepstorff P, Inagaki N, Shootinl: A protein involved in the organization of an asymmetric signal for neuronal polarization., J. Cell Biol 175 (2006) 147–57. doi:10.1083/jcb.200604160. [PubMed: 17030985]

[18]. Zheng S, Alternative splicing programming of axon formation., Wiley Interdiscip Rev RNA. (2020). doi: 10.1002/wrna.1585.

[19]. Gattiker E Gasteiger, A. Bairoch, ScanProsite: a reference implementation of a PROSITE scanning tool., Appl. Bioinformatics 1 (2002) 107–8. [PubMed: 15130850]

[20]. Gouw M, Michael S, Samano-Sanchez H, Kumar M, Zeke A, Lang B, Bely B, Chemes LB, Davey NE, Deng Z, Diella F, Gurth CM, Huber AK, Kleinsorg S, Schlegel LS, Palopoli N, Roey KV, Altenberg B, Remenyi A, Dinkel H, Gibson TJ, The eukaryotic linear motif resource - 2018 update, Nucleic Acids Res. 46 (2018) D428–D434. doi:10.1093/nar/gkx1077. [PubMed: 29136216]

[21]. WeiB CL, Schultz J, Identification of divergent WH2 motifs by HMM-HMM alignments, BMC Res. Notes (2015). doi: 10.1186/s13104-015-0981-7.

[22]. Hansen SD, Mullins RD, VASP is a processive actin polymerase that requires monomeric actin for barbed end association, J. Cell Biol 191 (2010) 571–584. doi: 10.1083/jcb.201003014. [PubMed: 21041447]

[23]. Bieling P, Hansen SD, Akin O, Li T, Hayden CC, Fletcher DA, Mullins RD, WH2 and proline-rich domains of WASP- family proteins collaborate to accelerate actin filament elongation, EMBO J. 37 (2018) 102–121. doi: 10.15252/embj.201797039. [PubMed: 29141912]

[24]. Uruno T, Liu J, Zhang P, Fan YX, Egile C, Li R, Mueller SC, Zhan X, Activation of Arp2/3 complex-mediated actin polymerization by cortactin, Nat. Cell Biol (2001). doi: 10.1038/35060051.

[25]. Loomis PA, Kelly AE, Zheng L, Changyaleket B, Sekerkova G, Mugnaini E, Ferreira A, Mullins RD, Bartles JR, Targeted wild-type and jerker espins reveal a novel, WH2-domain-dependent way to make actin bundles in cells, J. Cell Sci (2006). doi:10.1242/jcs.02869.

[26]. Simm D, Hatje K, Kollmar M, Waggawagga: Comparative visualization of coiled-coil predictions and detection of stable single α-helices (SAH domains), Bioinformatics. 31 (2015) 767–769. doi:10.1093/bioinformatics/btu700. [PubMed: 25338722]

[27]. Shimada T, Toriyama M, Uemura K, Kamiguchi H, Sugiura T, Watanabe N, Inagaki N, Shootinl interacts with actin retrograde flow and L1-CAM to promote axon outgrowth, J. Cell Biol (2008). doi: 10.1083/jcb.200712138.

[28]. rang Lin J, Hu J, SeqNLS: nuclear localization signal prediction based on frequent pattern mining and linear motif scoring., PLoS One. 8 (2013). doi: 10.1371/journal.pone.0076864.

[29]. Cyert MS, Regulation of Nuclear Localization during Signaling, J. Biol. Chem (2001). doi: 10.1074/jbe.R100012200.

[30]. Qualmann B, Kessels MM, New players in actin polymerization - WH2-domain-containing actin nucleators, Trends Cell Biol. 19 (2009) 276–285. doi: 10.1016/j.tcb.2009.03.004. [PubMed: 19406642]

[31]. Dominguez R, The WH2 Domain and Actin Nucleation: Necessary but Insufficient, Trends Biochem. Sci. 41 (2016) 478–490. doi: 10.1016/j.tibs.2016.03.004. [PubMed: 27068179]

[32]. Lappalainen P, Actin-binding proteins: The long road to understanding the dynamic landscape of cellular actin networks, Mol. Biol. Cell 27 (2016) 2519–2522. doi: 10.1091/mbc.E15-10-0728. [PubMed: 27528696]

[33]. Chereau D, Dominguez R, Understanding the role of the G-actin-binding domain of Ena/VASP in actin assembly., J. Struct. Biol 155 (2006) 195–201. doi:10.1016/j.jsb.2006.01.012. [PubMed: 16684607]

[34]. Havrylenko S, Noguera P, Abou-Ghali M, Manzi J, Faqir F, Lamora A, Guerin C, Blanchoin L, Plastino J, WAVE binds Ena/VASP for enhanced Arp2/3 complex-based actin assembly, Mol. Biol. Cell 26 (2015) 55–65. doi: 10.1091/mbc.E14-07-1200. [PubMed: 25355952]

[35]. Hofmann WA, Stojiljkovic L, Fuchsova B, Vargas GM, Mavrommatis E, Philimonenko V, Kysela K, Goodrich JA, Lessard JL, Hope TJ, Hozak P, de Lanerolle P, Actin is part of pre-initiation complexes and is necessary for transcription by RNA polymerase II., Nat. Cell Biol 6 (2004) 1094–101. doi: 10.1038/ncb1182. [PubMed: 15502823]

[36]. Sjolinder M, Bjork P, Soderberg E, Sabri N, Farrants A-KO, Visa N, The growing pre-mRNA recruits actin and chromatin-modifying factors to transcriptionally active genes., Genes Dev. 19 (2005) 1871–84. doi:10.1101/gad.339405. [PubMed: 16103215]

[37]. Zheng B, Han M, Bernier M, Wen JK, Nuclear actin and actin-binding proteins in the regulation of transcription and gene expression, FEBS J. 276 (2009) 2669–2685. doi: 10.1111/j.1742-4658.2009.06986.x. [PubMed: 19459931]

[38]. Belin BJ, Lee T, Mullins RD, DNA damage induces nuclear actin filament assembly by formin-2 and spire-1/2 that promotes efficient DNA repair, Elife. 4 (2015). doi: 10.7554/eLife.07735.

[39]. Zheng L, Beeler DM, Bartles JR, Characterization and regulation of an additional actin-filament-binding site in large isoforms of the stereocilia actin-bundling protein espin., J. Cell Sci 127 (2014) 1306–17. doi: 10.1242/jcs.143255. [PubMed: 24424026]

[40]. Heimsath EG, Higgs HN, The C terminus of formin FMNL3 accelerates actin polymerization and contains a WH2 domain-like sequence that binds both monomers and filament barbed ends, J. Biol. Chem (2012). doi: 10.1074/jbc.M111.312207.

[41]. Lammers M, Rose R, Scrima A, Wittinghofer A, The regulation of mDial by autoinhibition and its release by Rho*GTP, EMBO J. (2005). doi: 10.1038/sj.emboj.7600879.

[42]. Wakayama Y, Fukuhara S, Ando K, Matsuda M, Mochizuki N, Cdc42 mediates Bmp - Induced sprouting angiogenesis through Fmnl3-driven assembly of endothelial filopodia in zebrafish, Dev. Cell (2015). doi:10.1016/j.devcel.2014.11.024.

[43]. Campellone KG, Welch MD, A nucleator arms race: cellular control of actin assembly., Nat. Rev. Mol. Cell Biol 11 (2010) 237–51. doi:10.1038/nrm2867. [PubMed: 20237478]

[44]. Bompard G, Caron E, Regulation of WASP/WAVE proteins: Making a long story short, J. Cell Biol (2004). doi:10.1083/jcb.200403127.

[45]. Kubo Y, Baba K, Toriyama M, Minegishi T, Sugiura T, Kozawa S, Ikeda K, Inagaki N, Shootinl-cortactin interaction mediates signal-force transduction for axon outgrowth, J. Cell Biol 210 (2015) 663–676. doi: 10.1083/jcb.201505011. [PubMed: 26261183]

[46]. Sapir T, Levy T, Kozer N, Shin I, Zamor V, Haffner-Krausz R, McGlade JC, Reiner O, Notch activation by shootinl opposing activities on 2 ubiquitin ligases, Cereb. Cortex (2018). doi:10.1093/cercor/bhx180.

[47]. Gordon DJ, Boyer JL, Korn ED, Comparative biochemistry of non muscle actins, J. Biol. Chem (1977).

[48]. Huang S, Robinson RC, Gao LY, Matsumoto T, Brunet A, Blanchoin L, Staiger CJ, Arabidopsis VILLIN1 generates actin filament cables that are resistant to depolymerization, Plant Cell. (2005). doi: 10.1105/tpc.104.028555.

[49]. Kovar DR, Staiger CJ, Weaver EA, McCurdy DW, AtFiml is an actin filament crosslinking protein from Arabidopsis thaliana, Plant J. (2000). doi: 10.1046/j.1365-313X.2000.00907.X.

[50]. Liu G, Grant WM, Persky D, Latham VM, Singer RH, Condeelis J, Interactions of elongation factor 1a with F-actin and β-actin mRNA: Implications for anchoring mRNA in cell protrusions, Mol. Biol. Cell (2002). doi:10.1091/mbc.01-03-0140.

[51]. Sievers F, Wilm A, Dineen D, Gibson TJ, Karplus K, Li W, Lopez R, McWilliam H, Remmert M, Soding J, Thompson JD, Higgins DG, Fast, scalable generation of high-quality protein multiple sequence alignments using Clustal Omega, Mol. Syst. Biol 7 (2011). doi:10.1038/msb.2011.75.

[52]. Crooks G, Hon G, Chandonia J, Brenner S, WebLogo: a sequence logo generator, Genome Res. 14 (2004) 1188–1190. doi: 10.1101/gr.849004.1. [PubMed: 15173120]

[53]. Papadopoulos JS, Agarwala R, COBALT: constraint-based alignment tool for multiple protein sequences., Bioinformatics. 23 (2007) 1073–9. doi: 10.1093/bioinformatics/btm076. [PubMed: 17332019]

[54]. Bienert S, Waterhouse A, De Beer TAP, Tauriello G, Studer G, Bordoli L, Schwede T, The SWISS-MODEL Repository-new features and functionality, Nucleic Acids Res. 45 (2017) D313–D319. doi:10.1093/nar/gkw1132. [PubMed: 27899672]

[55]. Wang J, Youkharibache P, Zhang D, Lanczycki CJ, Geer RC, Madej T, Phan L, Ward M, Lu S, Marchler GH, Wang Y, Bryant SH, Geer LY, Marchler-Bauer A, iCn3D, a web-based 3D viewer for sharing 1D/2D/3D representations of biomolecular structures, Bioinformatics. (2019). doi: 10.1093/bioinformatics/btz502.

Highlights

- SHTN1 has a noncanonical WH2 domain for actin binding.

- The SHTN1 short isoform exhibits no actin-binding activity.

- A putative coiled-coil domain autoinhibits actin-binding activity of SHTN1 isoforms.

- SHTN1 uses alternative splicing instead of a third protein to relieve autoinhibition.
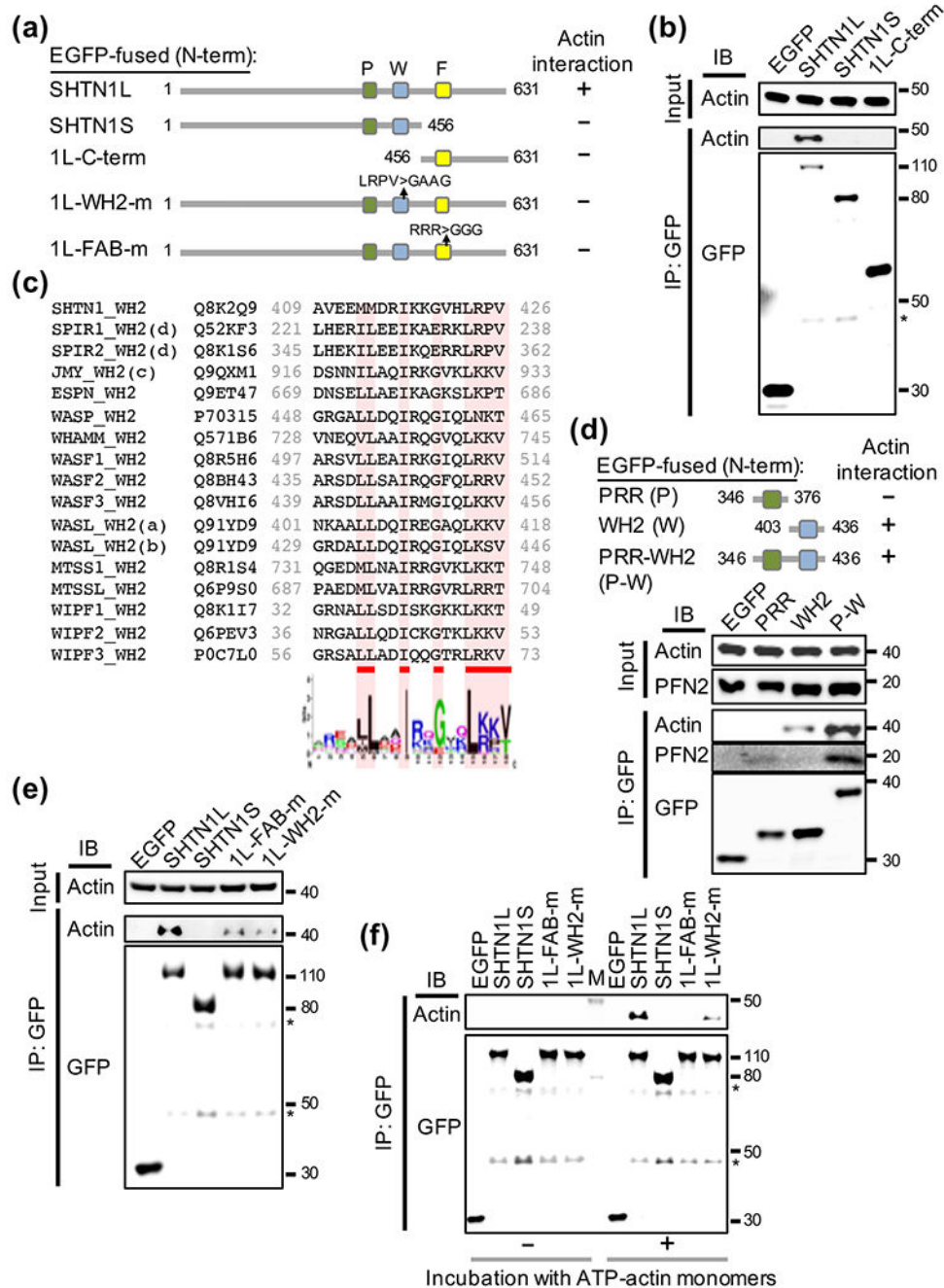
Fig. 1. Identification of a WH2 domain and a PRR domain in SHTN1.
(a) Diagram of EGFP-fused expression vectors. P, proline-rich region (PRR); W, WH2 domain; F, F-actin binding site (FAB). **(b)** Immunoblot (IB) analysis of cellular actin co-IPed with EGFP-fused SHTN1 proteins. IP: immunoprecipitation. **(c)** Clustal Omega [51] alignment of WH2 domain sequences from mouse ABPs listed by their names and UniProt IDs. Critical residues are underlined. Amino acid frequencies are shown as a WebLogo output [52]. **(d)** Schematic of P, W, and P-W domain constructs, and their actin-binding abilities. Blots of lysate inputs and co-IP proteins were probed for ACTB, PFN2, and GFP.

(e) IB analysis of endogenous actin co-IPed with EGFP-fused SHTN1 variants. **(f)** IB analysis of G-actin binding assay to detect ATP-actin monomers captured by EGFP-fusion proteins immobilized on GFP-Trap beads. EGFP-fused SHTN1S and SHTN1L migrate at 80 kDa and 110 kDa, respectively, on SDS-PAGE. Asterisks (*) denote degradation products.
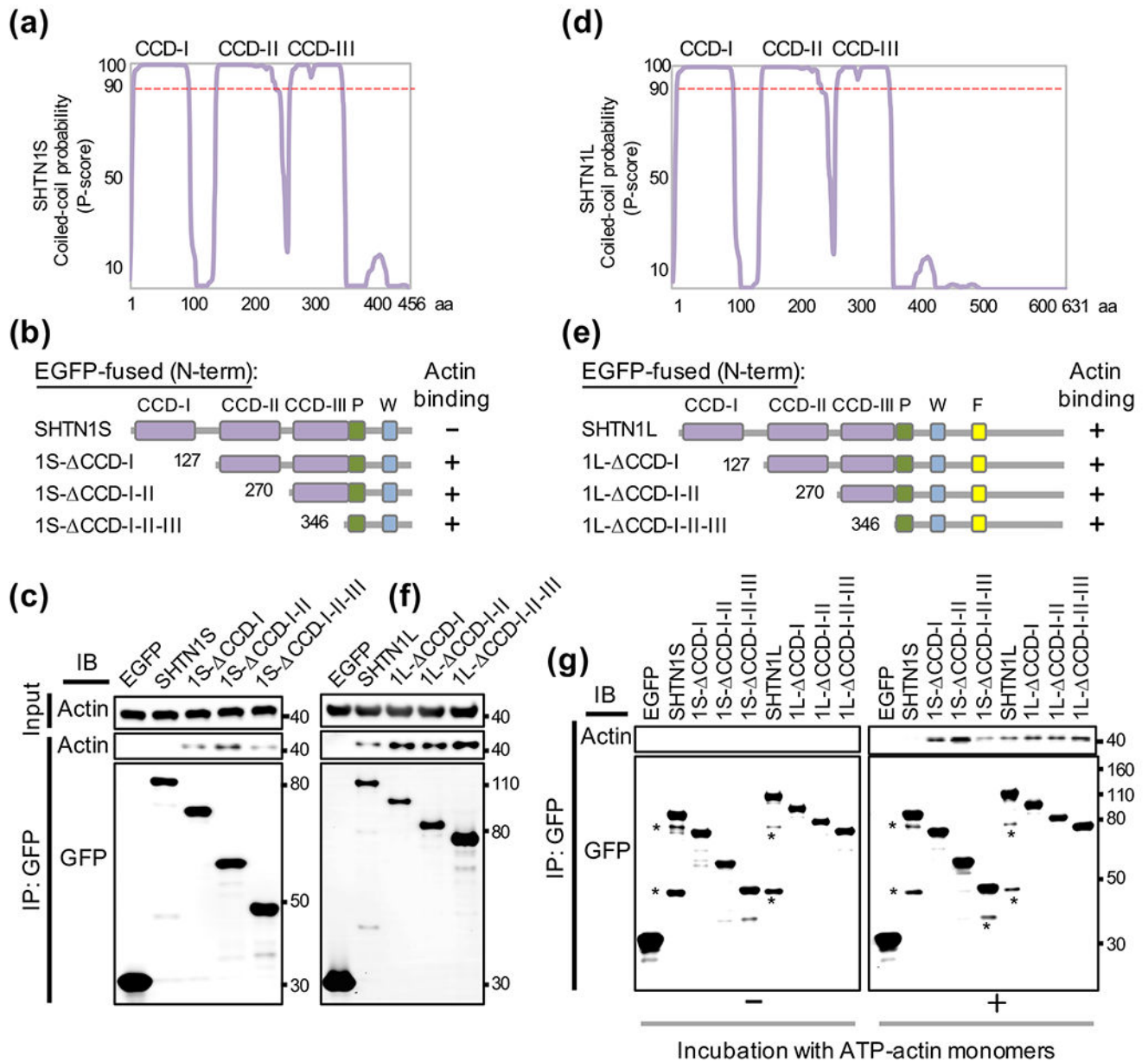
Fig. 2. CCDs inhibit WH2-actin interaction.
(a) and (d) The putative coiled-coil profiles of SHTN1S and SHTN1L predicted by Marcoil [26]. The vertical scale is the CCD probability between 0 and 100 and the horizontal scale shows the amino acid numbers. Regions of high probability scores above 90% with 21-residue window size are classified as CCD. (b) and (e) Schematics of SHTN1 domain structures and CCD mutants fused to EGFP, and their abilities to interact with actin. (c) Immunoblot (IB) data shows actin is co-IPed with 1S-CCD mutants, but not full-length SHTN1S. (f) IB analysis shows endogenous actin co-IPed with SHTN1L and its CCD mutants, (g) IB analysis of G-actin binding assay to detect ATP-bound actin monomers captured by EGFP-fusion proteins immobilized on GFP-Trap beads. Asterisks (*) denote degradation products.
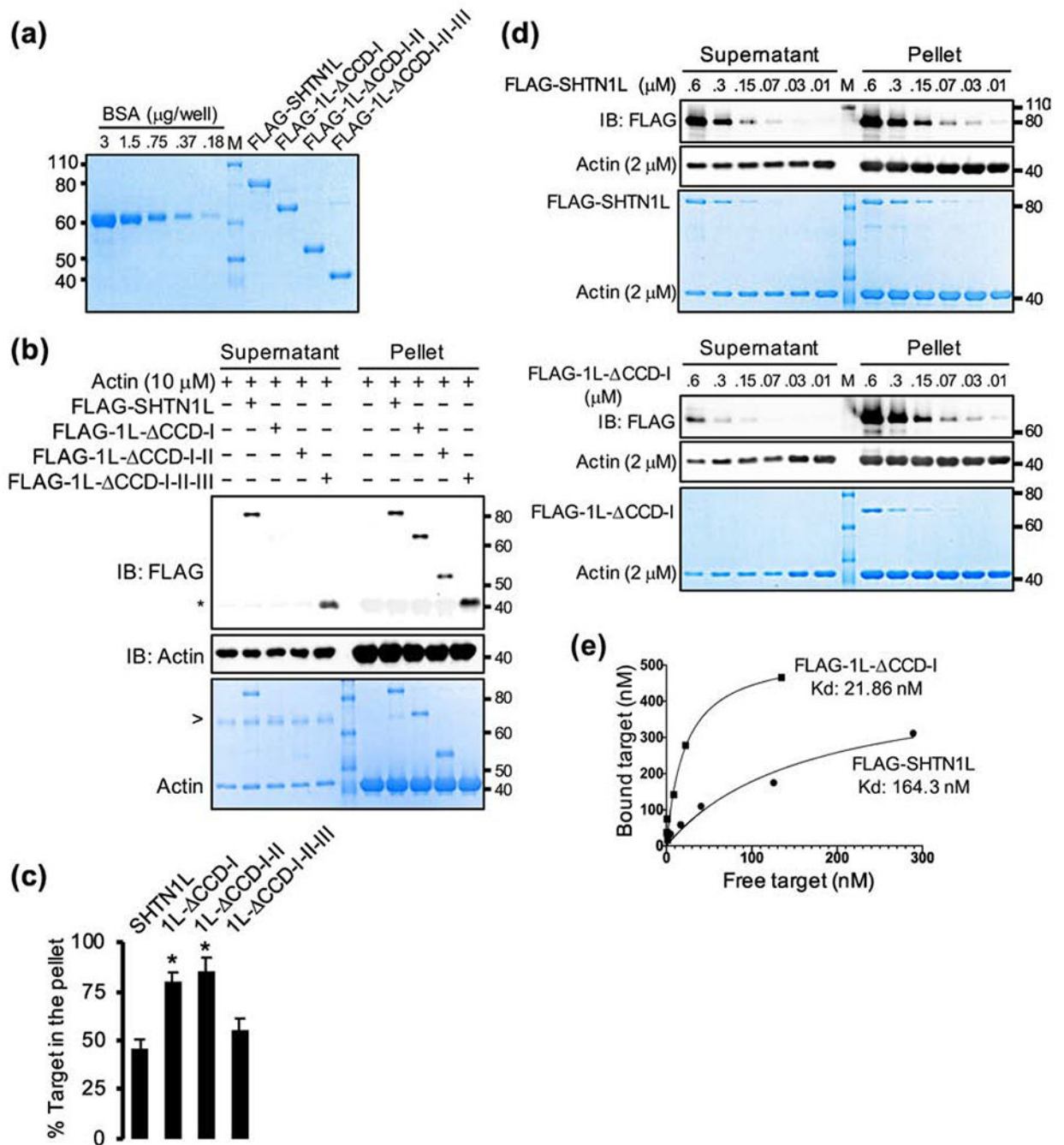
Fig. 3. CCD-I suppresses SHTN1L's activity of binding F-actin.
(a) Coomassie blue-stained gel image shows the purity of FLAG-tagged target proteins. (b) Cosedimentation experiments were performed using 10 μM actin alone or with 250 nM purified FLAG-tagged SHTN1L variants. Pellet and supernatant fractions were resolved and immunoblotted (IB) with anti-FLAG and anti-β-actin Abs (upper panels) or stained with Coomassie blue (lower panel). Asterisk (*) denotes the faint bands of background actin molecules, which co-migrates with 1L- CCD-I-II-III mutant proteins. Arrowhead (>) in Coomassie blue-stained SDS-PAGE depicts occasionally observed impurities from the actin

stock, **(c)** Bar graph shows the fraction of test molecules in the pellet. Data represent mean ± SEM. * p<0.05. **(d)** Cosedimentation assays were carried out to determine the interaction of F-actin (2 μM) with FLAG-tagged SHTN1L or 1L- CCD-I starting with a final concentration of 0.6 μM in a 40 μl reaction volume. Equal amounts of the supernatant and pellet fractions were loaded in each lane and the targets were detected by Coomassie blue-staining and immunoblotting with anti-FLAG and anti-b-actin Abs. **(e)** The concentration of bound targets was plotted against the concentration of free target molecules as previously described [48,49]. The *Kd* for SHTN1L and 1L- CCD-I are 164.3 nM (95% CI: 49.32-1376 nM; Bmax: 469.8 nM) and 21.86 nM (95% CI: 9.51-49.93 nM; Bmax: 540.7 nM), respectively. The amounts of test molecules were quantified using fluorescence immunoblot images. Images were acquired without signal saturation and pixel intensities of target bands were within the dynamic range of Typhoon scanning. Densitometric analysis of target bands were assessed to assure the signal intensities were linearly correlated with the amount of loaded proteins (R2: 0.95 ±0.15)
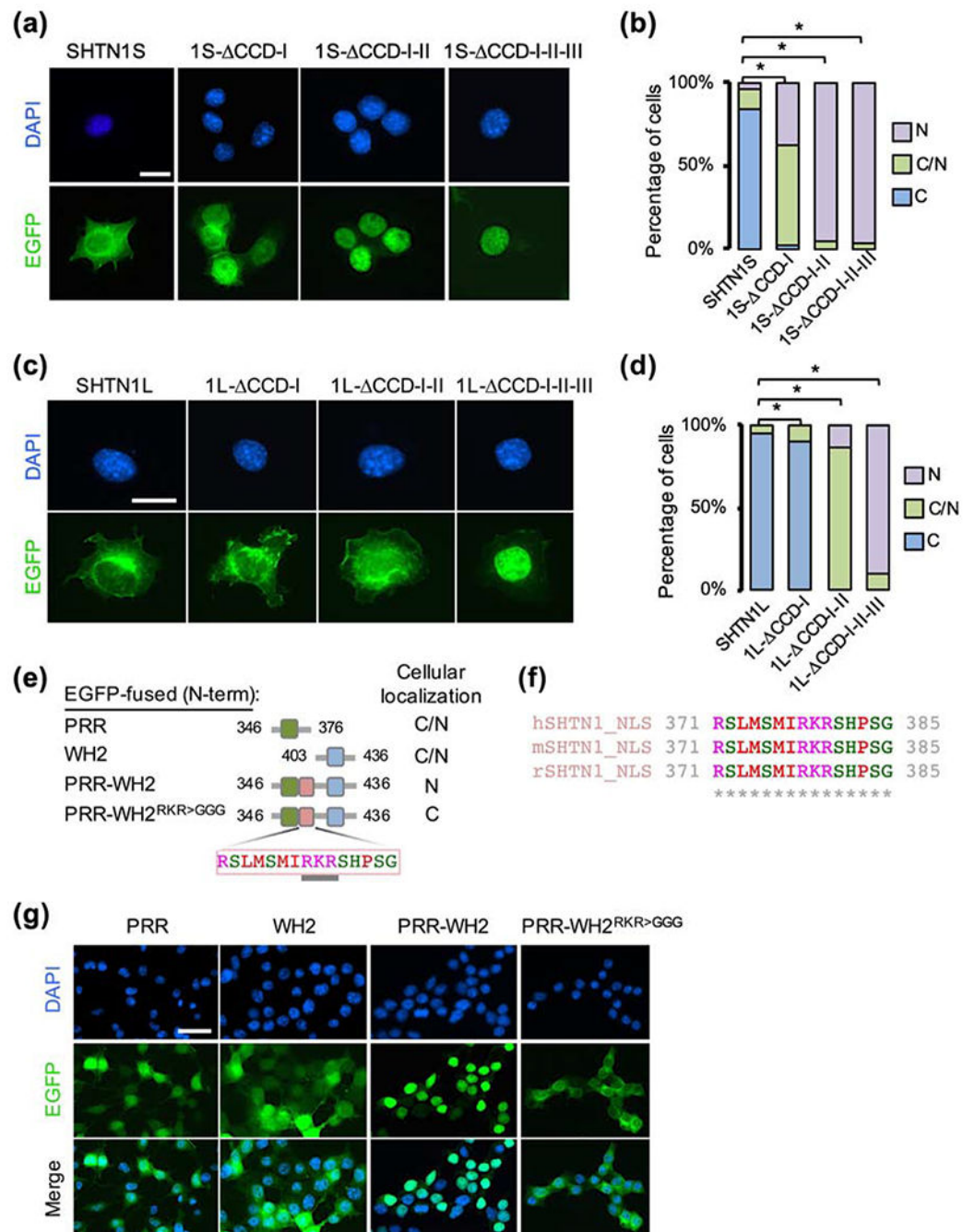
Fig. 4. Identification of a hidden NLS in SHTN1.

(**a**) and (**c**) Cellular localization of WT and mutant variants in N2a cells, (**b**) and (**d**) Graphs depict quantification of differential localization. 200 cells per condition, N=2. Fisher's exact test, * $p < 0.05$. Scale bar, 10 μm. C, cytoplasm; C/N, distributed in cytoplasm and nucleus; N, nucleus, (**e**) Schematics for EGFP-fused vectors and their cellular localization. PRR-WH2$^{RKR>GGG}$ depicts the putative NLS and mutated residues (underlined), (**f**) Alignment of the predicted NLS among human and rodents. Asterisks denote conserved

residues, (g) EGFP-tagged WT and mutated constructs were transiently expressed in N2a cells, and immunostained with anti-GFP pAb. Scale bar, 10 μm.